Articles

Main Chain and Side Chain Dynamics of a Heme Protein: ^{15}N and ^{2}H NMR Relaxation Studies of *R. capsulatus* Ferrocytochrome c_2[†]

Peter F. Flynn, Ramona J. Bieber Urbauer,[‡] Hui Zhang, Andrew L. Lee,[§] and A. Joshua Wand*

The Johnson Research Foundation and Department of Biochemistry and Biophysics, University of Pennsylvania, Philadelphia, Pennsylvania 19104-6059

Received February 2, 2001; Revised Manuscript Received March 14, 2001

ABSTRACT: A detailed characterization of the main chain and side chain dynamics in *R. capsulatus* ferrocytochrome c_2 derived from ^{2}H NMR relaxation of methyl group resonances is presented. ^{15}N relaxation measurements confirm earlier results indicating that *R. capsulatus* ferrocytochrome c_2 exhibits minor rotational anisotropy in solution. The current study is focused on the use of deuterium relaxation in side chain methyl groups, which has been shown to provide a detailed and accurate measure of internal dynamics. Results obtained indicate that the side chains of ferrocytochrome c_2 exhibit a wide range of motional amplitudes, but are more rigid than generally found in the interior of nonprosthetic group bearing globular proteins. This unusual rigidity is ascribed to the interactions of the protein with the large heme prosthetic group. This observation has significant implications for the potential of the heme−protein interface to modulate the redox properties of the protein and also points to the need for great precision in the design and engineering of heme proteins.

Cytochrome c_2 functions as a soluble electron carrier between membrane-bound redox centers under both photosynthetic and respiratory growth conditions. Cytochrome c_2 is a member of the class I cytochromes *c*, which are characterized by covalent attachment of the *c*-type heme moiety to the protein via a CXXCH binding motif. The family of cytochromes c_2 exhibits a larger range of redox potentials (250−450 mV) than that of cytochromes *c* (250−270 mV), and the redox potential for *Rhodobacter capsulatus* c_2 has been determined to be 350 mV. The crystal (*1*) and solution (*2*) structures of ferrocytochrome c_2 show that it is composed of five helical regions connected by structured loops and a classical methionine-histidine axial heme ligation scheme. Residues 3 through 16 compose helix-1, residues 55 through 63 make up helix-2, residues 69 through 77 make up helix-3, residues 80 through 87 constitute helix-4, and helix-5 is composed of residues 104 through 114. Two type-I turns are formed from residues 21 through 24 and from residues 89 to 91, and two type-II turns are formed from residues 37 to 40 and from residues 40 through 43. There are no significant differences between the crystal (*1*) and solution (*2*) structures.

No direct structural comparison of the reduced and oxidized states of cytochromes c_2 has yet been accomplished. Prior studies of homologous *c*-type cytochromes reveal that the reduced and oxidized forms of cytochrome *c* differ in a number of chemical and physical properties (*3*−*10*). Remarkably, however, the comparison of the crystal structures of the redox pairs of tuna (*11, 12*) and yeast (*13*) indicates that only relatively subtle structural differences exist. Solution NMR[1] studies designed to monitor redox-state-dependent chemical shift changes in horse-heart cytochrome *c* likewise suggest that only small structural changes are associated with the change in oxidation state (*14*−*17*). Complete NMR assignment of the ^{1}H, ^{13}C, and ^{15}N resonances of the reduced form of *R. cap*s cytochrome c_2 has been accomplished (*18*−*21*), including ^{1}H and ^{13}C resonances of the heme group.

[†] Supported by NIH Grant GM35940 and by equipment grants from the NIH and the ARO.

* Address correspondence to this author at the Department of Biochemistry and Biophysics, University of Pennsylvania, Philadelphia, PA 19104. Telephone: (215)-573-7288, facsimile: (215)-573-7290, e-mail: wand@mail.med.upenn.edu.

[‡] Present address: Department of Molecular Biosciences, 7042 Haworth Hall, 1200 Sunnyside, University of Kansas, Lawrence, KS 66045-7534.

[§] Present address: Division of Medicinal Chemistry and Natural Products, School of Pharmacy, CB# 7360, Beard Hall, University of North Carolina at Chapel Hill, Chapel Hill, NC 27599-7360.

[1] Abbreviations: CPMG, Carr−Purcell−Meiboom−Gill; $D_{\parallel}/D_{\perp}$, ratio of diffusion coefficients parallel and perpendicular to the principal axis of the rotational diffusion tensor; $\Delta\sigma$, value of the chemical shift anisotropy; e^2qQ/h, quadrupolar coupling constant; HSQC, heteronuclear single-quantum coherence; I_zC_z, two-spin longitudinal proton and carbon coherence; $I_zC_zD_z$, three-spin longitudinal proton, carbon, and deuterium coherence; $I_zC_zD_y$, three-spin longitudinal proton and carbon coherence with transverse deuterium coherence; $J(\omega)$, power spectral density function; NMR, nuclear magnetic resonance; NOE, nuclear Overhauser effect; *R. caps*, *Rhodobacter capsulatus*; S^2, squared generalized order parameter; S^2_{axis}, squared generalized order parameter for the symmetry axis between the methyl carbon and its adjacent carbon; T_1, longitudinal or spin−lattice relaxation time constant; $T_{1\rho}$, spin-locked relaxation time constant; T_2, transverse or spin−spin relaxation time constant; τ_m, global correlation time; τ_e, correlation time for internal motion.

10.1021/bi0102252 CCC: $20.00
Published on Web 05/09/2001

Thus, cytochrome c_2 is well positioned as a candidate for extensive characterization of its internal dynamics by NMR-based methods.

Over the past decade, solution NMR relaxation studies of proteins have largely focused on main chain resonances, i.e., the N^H, C^α, and C′ nuclei (e.g, *22*−*28*). These studies have established that the main chains of native proteins, as characterized by the behavior of amide N−H bond vectors, are generally highly restricted in the amplitude of subnanosecond motion in regions of regular secondary structure. More recently, technical developments have allowed the use of both ^{13}C-based (*29*−*31*) and ^{2}H-based (*32*) NMR relaxation methods to characterize the dynamics of side chains within globular proteins of significant size. A general theme emerging from NMR relaxation studies of methyl-bearing side chains of proteins is that the hydrophobic cores of natural proteins are quite dynamic and heterogeneously so (*30, 31, 33*−*37*). Furthermore, it has been suggested that the subnanosecond time scale motions of methyl-bearing side chains in native proteins tend to cluster into three distinct classes of angular order (*38*). The origin of this distribution has not yet been revealed, but one would anticipate that is intimately related to the details of close packing within the interior of the protein molecule. In this respect, proteins bearing large inflexible prosthetic groups, such as heme or flavin, are naturally of interest. It is not at all clear how the presence of extensive noncovalent and covalent interactions between the prosthetic group and the protein will change the fundamental dynamic properties of the protein. The general purpose of the work described here was to investigate the general dynamic properties of a heme−protein complex. Characterization of the dynamic properties of such complexes is clearly important to a quantitative understanding of their stability, through the corresponding residual entropy (*39, 40*), and to redox function (*41*−*43*). Here we present a quantitative examination of the internal dynamics of ferrocytochrome c_2, a representative member of an important class of heme proteins, using ^{2}H NMR relaxation of side chain methyl resonances. The results obtained indicate that the motional side chains in ferrocytochrome c_2 exhibit a wide range of amplitudes, but are generally more rigid than generally found in the interior of nonprosthetic group bearing globular proteins. This observation has significant implications for the potential of the heme−protein interface to modulate the redox properties of the protein and may identify the origin of the apparent difficulty in the *de novo* design of optimally structured heme proteins (*44*).

EXPERIMENTAL PROCEDURES

Sample Preparation. Cytochrome c_2 from *Rhodobacter capsulatus* was expressed and purified using protocols adapted from previous work (*18, 21*). Samples enriched in ^{2}H, ^{13}C, and ^{15}N were produced from cells grown on media containing 50% H_2O, 50% D_2O, $^{15}NH_4Cl$ (U-^{15}N, 98%), and D-glucose (U-$^{13}C_6$, 99%) as the sole nitrogen and carbon sources, respectively, from which protein uniformly labeled in ^{15}N and ^{13}C and randomly fractionally deuterated to 30−40% was obtained. The level of fractional deuteration was estimated based on intensities of cross-peaks arising from the individual isotopomers (-CH_3, -CH_2D, -CHD_2) present in the ^{2}H-decoupled ^{13}C-HSQC spectrum. The protein samples were dissolved in a solution of 90% H_2O, 10% D_2O, 50 mM potassium phosphate, pH 6.0. The protein concentrations of both ^{15}N-labeled and ^{2}H-, ^{13}C-, and ^{15}N-labeled samples were 0.8 mM. The latter sample (300 μL) was prepared in a Shigemi Microcell NMR tube (Shigemi, Inc., Allison Park, PA).

NMR Spectroscopy. NMR relaxation experiments were conducted on Varian Unity Inova spectrometers equipped with ^{1}H/^{13}C,^{15}N probes and triple-axis pulsed-field gradient accessories. All relaxation experiments were carried out at 30 ± 0.5 °C, as determined using a methanol standard (Wilmad) (*45*). ^{1}H, ^{15}N, and ^{13}C NMR assignments (including assignment of heme resonances) were derived from previously published research (*18, 19, 21*). Stereospecific assignments of the methyl groups of leucine and valine could not be obtained using the labeling approach of Neri et al. (*46*) due to the difficulty associated with growth and expression of the protein when utilizing glucose as a sole carbon source.

Longitudinal (T_1) and transverse (T_2) relaxation of ^{15}N nuclei was measured at 11.7 and 14.1 T, corresponding to ^{15}N Larmor frequencies of 50.6 and 60.87 MHz, respectively, using a pulse sequence based on the ^{15}N-HSQC experiment (*47*, *48*). The {^{1}H}-^{15}N NOE was also measured at 11.7 and 14.1 T, based on a ^{1}H/^{15}N correlation experiment recorded with and without broadband ^{1}H saturation that produces a change in the intensity of ^{1}H-^{15}N cross-peaks due to the nuclear Overhauser effect (*22*). The experiment to measure longitudinal relaxation employed a cycling scheme based on the Freeman−Hill approach wherein signal intensities vary from unity to zero (*49*). Cross-correlated relaxation during longitudinal relaxation was eliminated by applying 120° ^{1}H pulses every 5 ms. Cross-correlation effects during transverse relaxation were eliminated by applying ^{15}N 180° pulses in the CPMG train every 900 μs, and by applying ^{1}H 180° pulses that were centered in the CPMG module (*48*). Recycle delays in the NOE, T_1, and T_2 experiments were 2.0, 1.5, and 2.0 s, respectively. Pulse sequences used to record ^{15}N NMR relaxation data employed sensitivity-enhanced gradient selection of ^{15}N coherence (*50*).

Longitudinal ^{15}N NMR relaxation experiments at 50.6 and 60.87 MHz employed relaxation delay times of 50, 85, 120, 190, 270, 350.0, 440. 540, 750, 880, 1000, 1200, and 1500 ms. Transverse ^{15}N NMR relaxation experiments at 50.6 MHz employed a RF field-strength of 5.4 kHz (^{15}N 90° pulse of 46 μs) and relaxation delay times of 7.94*, 15.87, 23.81, 31.74, 39.68, 47.62, 63.49, 79.36*, 95.23, 103.17*, 119.04, 134.91, and 142.82 ms, where asterisks indicate duplicate measurements. Transverse ^{15}N NMR relaxation experiments at 60.87 MHz employed a RF field-strength of 7.4 kHz and relaxation delay times of 7.74*, 15.49, 23.23, 30.98, 38.72, 46.46*, 54.21, 61.95, 77.44, 92.92, 108.42, and 131.65* ms.

Experiments at 50.6 MHz were recorded using 128 complex incremented time domain (^{15}N) points and 1024 complex real-time (^{1}H) points, respectively, with the ^{1}H carrier frequency set at the H_2O frequency, ∼4.7 ppm, and the ^{1}H spectral width set at 16.01 ppm (8000 Hz); the ^{15}N carrier frequency was set at 119 ppm, and the ^{15}N spectral width was set at 41.17 ppm (2262 Hz). Experiments at 60.78 MHz were recorded using 128 complex t_1 (^{15}N) points and 1024 complex t_2 (^{1}H) points, respectively, with the ^{1}H carrier frequency set at the H_2O frequency and the ^{1}H spectral width set at 9400 Hz; the ^{15}N carrier frequency was set at 119 ppm, and the ^{15}N spectral width was set at 2500 Hz.

Deuterium NMR relaxation was characterized using experiments that measure relaxation of multiple spin coherences involving longitudinal proton and carbon coherence, $R(I_zC_z)$; longitudinal proton, carbon, and deuterium coherence, $R(I_zC_zD_z)$; and longitudinal proton and carbon nuclei with transverse deuterium coherence, $R(I_zC_zD_y)$ (*32*). Static field strengths of 11.7 and 14.1 T were used, producing ^{2}H Larmor frequencies of 76.7 and 92 MHz, respectively. Deuterium NMR relaxation experiments at 76.7 MHz employed relaxation delay times of 1.0*, 11.2, 22.4, 33.6*, 44.8, 56.0, 67.2, 78.5*, and 90.0 ms for I_zC_z; 3.0*, 8.0*, 15.0, 25.0, 35.0, 45.0, 55.0, 65.0, and 80.0 ms for $I_zC_zD_z$; and 1.0*, 3.0*, 5.0, 7.0, 10.0, 13.0, 17.0, 20.0*, and 25.0 ms for $I_zC_zD_y$. Recycle delay times of 1.8, 1.8, and 2.1 s were employed, and 64, 112, and 112 transients per free induction decay were used for I_zC_z, $I_zC_zD_z$, and $I_zC_zD_y$, respectively. Experiments at 76.7 MHz were recorded using 62 complex t_1 (^{13}C) points and 1024 complex t_2 (^{1}H) points, respectively, with the ^{1}H carrier frequency set at 4.7 ppm and the ^{1}H spectral width set at 9997 Hz; the ^{13}C carrier frequency was set at 18.85 ppm, and the ^{13}C spectral width was set at 2262 Hz. Deuterium NMR relaxation experiments at 92 MHz employed relaxation delay times of 1.0*, 11.2, 22.4, 33.6*, 44.8, 56.0, 67.2, 78.5*, and 90.0 ms for I_zC_z; 3.0*, 8.0*, 15.0*, 25.0*, 35.0, 45.0, 55.0, 65.0*, and 80.0 ms for $I_zC_zD_z$; and 1.0*, 3.0*, 5.0, 7.0, 10.0, 13.0, 17.0, 20.0*, and 25.0 ms for $I_zC_zD_y$. Recycle delay times of 1.8, 1.8, and 2.1 s were employed, and 64, 112, and 112 transients per free induction decay were used for I_zC_z, $I_zC_zD_z$, and $I_zC_zD_y$, respectively. Experiments at 92 MHz were recorded using 75 complex t_1 (^{13}C) points and 1024 complex t_2 (^{1}H) points, respectively, with the ^{1}H carrier frequency set at 4.7 ppm and the proton spectral width set 12 000 Hz, with the ^{13}C carrier frequency set at 18.85 ppm and the carbon spectral width set at 2715 Hz.

^{15}N Relaxation Data Analysis. ^{15}N NMR relaxation was analyzed using contributions from dipole−dipole and chemical shift anisotropy relaxation mechanisms (*51*):

$$\frac{1}{T_1} = \left(\frac{\hbar^2\gamma_H^2\gamma_N^2}{4r_{HN}^2}\right)[J(\omega_H - \omega_N) - 3J(\omega_N) + 6J(\omega_H + \omega_N)] + \frac{\omega_N^2\Delta\sigma^2}{3}J(\omega_N) \quad (1)$$

$$\frac{1}{T_2} = \left(\frac{\hbar^2\gamma_H^2\gamma_N^2}{8r_{HN}^2}\right)[4J(0) + J(\omega_H - \omega_N) - 3J(\omega_N) + 6J(\omega_H) + 6J(\omega_H + \omega_N)] + \frac{\omega_N^2\Delta\sigma^2}{3}[4J(0) + 3J(\omega_N)] \quad (2)$$

$$\mathrm{NOE} = 1 + \frac{\gamma_H}{\gamma_N}\left(\frac{\hbar^2\gamma_H^2\gamma_N^2}{4r_{HN}^6}\right)[6J(\omega_H + \omega_N) - J(\omega_H - \omega_N)] \quad (3)$$

where γ_I and ω_I are the gyromagnetic ratio and Larmor frequency of spin I, $\Delta\sigma$ ($\sigma_{||} - \sigma_\perp$) is the value of the axially symmetric ^{15}N chemical shift anisotropy, and r_{NH} is the N−H bond distance. In addition, conformational exchange, designated R_{ex}, can also contribute to the rate of spin−spin relaxation.

^{2}H Relaxation Data Analysis. ^{2}H relaxation is dominated by this quadrupolar mechanism, which for an axially symmetric electric field gradient may be written as (*52*)

$$\frac{1}{T_1(D)} = \frac{3}{16}\left(\frac{e^2qQ}{\hbar^2}\right)[J(\omega_D) + 4J(2\omega_D)] \quad (4)$$

$$\frac{1}{T_{1\rho}(D)} = \frac{1}{32}\left(\frac{e^2qQ}{\hbar^2}\right)[9J(0) + 15J(\omega_D) + 6J(2\omega_D)] \quad (5)$$

where e^2qQ/h is the quadrupolar coupling constant and $J(0)$, $J(\omega_D)$, and $J(2\omega_D)$ correspond to the spectral density function evaluated at the zero, single-, and double-quantum ^{2}H frequencies. The principal axis of the electric field gradient tensor was generally assumed to be collinear with the C−D bond vector, although this assumption may not be completely accurate for methyl groups (*53*).

Simple Model Free Spectral Densities. The so-called model free treatment of Lipari and Szabo (*54*, *55*) of the spectral density, $J(\omega)$, has been employed. The model free spectral density for isotropic global tumbling is written as

$$J(\omega) = \frac{2}{5}\left[\frac{S^2\tau_m}{1 + \omega^2\tau_m^2} + \frac{S^2\tau}{1 + \omega^2\tau^2}\right] \quad (6)$$

where $\tau^{-1} = \tau_m^{-1} + \tau_e^{-1}$, the τ_e parameter is the effective correlation time for the internal motion, and S^2 is the squared generalized order parameter. For anisotropic global motion that is axially symmetric, the model free spectral density takes the form (*56*):

$$J(\omega) = S^2\left[\frac{A_1\tau_1}{1 + \omega^2\tau_1^2} + \frac{A_2\tau_2}{1 + \omega^2\tau_2^2} + \frac{A_3\tau_3}{1 + \omega^2\tau_3^2}\right] + (1 - S^2)\left[\frac{\tau}{1 + \omega^2\tau^2}\right] \quad (7)$$

where

$$A_1 = \frac{(3\cos^2\theta - 1)}{4};\ \tau_1 = \frac{1}{6D_\perp};$$

$$A_2 = 3\sin^2\theta\cos^2\theta;\ \tau_2 = \frac{1}{5D_\perp + D_{||}}$$

$$A_3 = \frac{3}{4}\sin^4\theta;\ \tau_3 = \frac{1}{2D_\perp + 4D_{||}}$$

$$\frac{1}{\tau} = 6\mathrm{D} + \frac{1}{\tau_e};\ D = \frac{1}{3}(2D_\perp + D_{||})$$

NMR Data Processing and Analysis. The time-domain data were processed into 1024 × 1024 (^{15}N relaxation data sets) or 512 × 1024 matrixes (^{2}H relaxation data sets) using Felix 97.0 software (Molecular Simulations Inc., San Diego). Digital resolution in the processed ^{15}N data sets was 3.9 and 2.3 Hz/point for the ^{1}H and ^{15}N dimensions, respectively, at 50.6 MHz, and 4.6 and 2.4 Hz/point for the ^{1}H and ^{15}N dimensions, respectively, at 60.78 MHz. Digital resolution in the processed ^{2}H relaxation data sets was 2 and 0.3 Hz/point, respectively, in the ^{1}H and ^{13}C dimensions.

Cross-peak intensities were used to quantitate cross-peaks in the ^{15}N and ^{2}H relaxation data sets, and the uncertainties in these intensities were estimated from consideration of duplicate measurements and the root-mean-squared noise level of the matrix base-plane. The Levenberg−Marquardt algorithm was used for nonlinear two-parameter curve-fits for all ^{15}N and ^{2}H relaxation data. The residual χ^2 values were generally less than or equal to the number of fitted time/intensity points, suggesting that the data were well fit. {^{1}H}-^{15}N NOEs were calculated from peak intensity ratios, I^{NOE}/I^{ref}, taken from the NOE (^{1}H saturation) and reference (without ^{1}H saturation) experiments. Intensity uncertainties for the NOE experiments were estimated based on the root-mean-square noise level in the base-plane.

Deconvolution of ^{2}H T_1 and $T_{1\rho}$ Parameters. Values of ^{2}H T_1 and $T_{1\rho}$ were deconvoluted from the measured relaxation rates of multiple-spin I_zC_z, I_zC_z, $I_zC_zD_z$, and $I_zC_zD_y$ coherences in the following manner (*32*):

$$R_1(D) = \frac{1}{T_1} = R(I_zC_zD_z) - R(I_zC_z) \quad (8)$$

$$R_{1\rho}(D) = \frac{1}{T_{1\rho}} = R(I_zC_zD_y) - R(I_zC_z) \quad (9)$$

Evaluation of Internal Dynamic Parameters. Internal dynamic parameters were determined using a local fit for each methyl site using a exhaustive grid search (*23*) or nonlinear least-squares Powell minimization of the error function:

$$\chi^2 = \sum_j^M \left(\frac{\text{obs}_j - \text{calc}_j}{\lambda_j^{\text{obs}}} \right)^2 \quad (10)$$

where for each spin j, obs$_j$ is the jth measured relaxation parameter, calc$_j$ is the jth calculated relaxation parameter, and λ_j^{obs} is the estimated uncertainty in obs$_j$ for all relaxation measurements, M, i.e., T_1, T_2, and NOE in the case of ^{15}N relaxation and T_1 and $T_{1\rho}$ in the case of ^{2}H relaxation. The chemical shift anisotropy, $\Delta\sigma$ ($\sigma_{||} - \sigma_{\perp}$), for ^{15}N was taken to be equal to −170 ppm, and the N−H bond length was taken to be equal to 1.02 Å. The quadrupolar coupling constant, e^2qQ/h, was taken to be 165 kHz (*57*). Parameter errors were estimated based on 150 Monte Carlo simulations.

RESULTS AND DISCUSSION

Ferrocytochrome c_2 Backbone Dynamics Derived from ^{15}N Relaxation. As a prelude to the study of side chain dynamics based on ^{2}H relaxation, the global tumbling of the protein must be characterized. The influence of anisotropic tumbling on model free parameters (*54*, *55*) derived from NMR relaxation has been extensively documented (*56*, *58*, *59*). To characterize global tumbling of ferrocytochrome *c*, we have employed a standard strategy that has been outlined in detail elsewhere (*60*). The time constant for global tumbling, τ_m, was first determined using an isotropic global tumbling model and employed ^{15}N NMR relaxation parameters (T_1, T_2, and NOE) obtained at two magnetic field strengths. The examples shown in Figure 1 illustrate the high quality of the primary relaxation data obtained. The best-fit value of τ_m according eq 10 was determined using an exhaustive grid search (*23*) to be 6.7 ns. The anisotropy of reorientation was then determined based on analysis of measured ^{15}N T_1 and T_2 parameters according to the procedure of Bax and coworkers (*56*). The rotational anisotropy, expressed as the ratio of diffusion coefficients parallel and perpendicular to the principal axis of the rotational diffusion tensor ($D_{||}/D_{\perp}$), wasfound to be 1.20. This slight anisotropy has a negligible effect on the obtained model free parameters describing internal motion in the molecule as demonstrated in Figure 2b.

The rotational diffusion anisotropy and backbone dynamics of reduced cytochrome c_2 have been previously examined using ^{15}N NMR relaxation methods under different solution

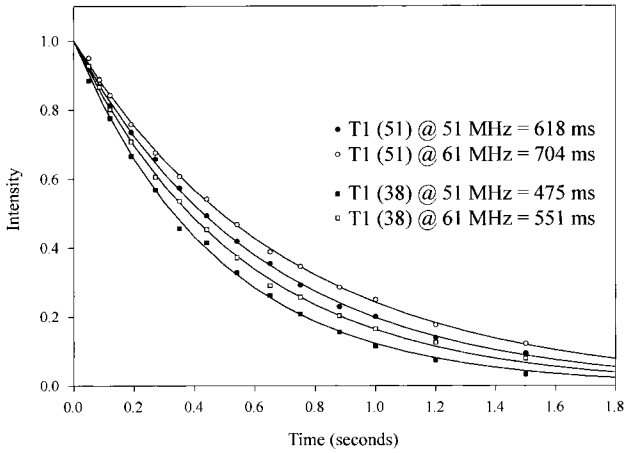

FIGURE 1: Examples of ^{15}N T_1 relaxation data recorded for ferrocytochrome c_2 at 50.6 and 60.87 MHz ^{15}N and 30 °C. Shown are data for residues 51 and 38. The solid lines are the fitted curves.

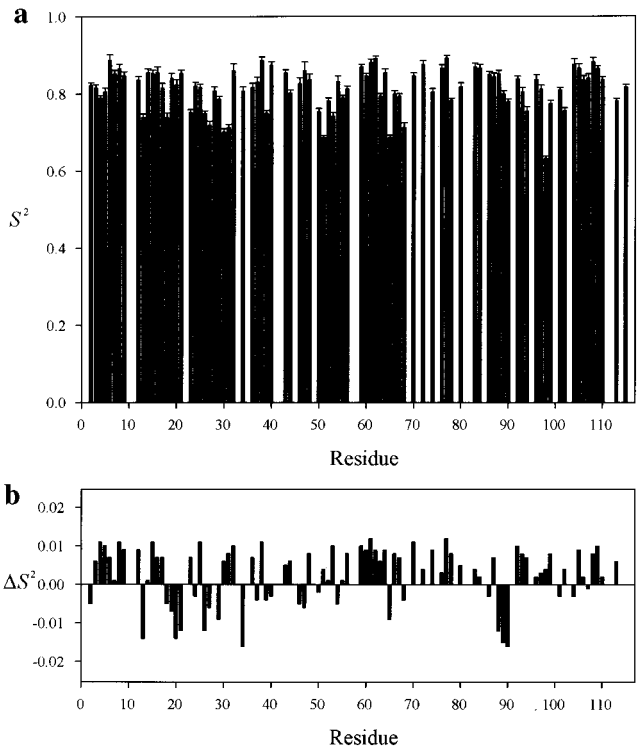

FIGURE 2: (a) Squared generalized order parameters (S^2) for the backbone amide N−H of ferrocytochrome c_2 derived from ^{15}N relaxation data recorded at 30 °C and analyzed using an axially symmetric diffusion tensor (see text). (b) Differences between S^2 parameters obtained using isotropic and axially symmetric diffusion tensors. $\Delta S^2 = S^2_{iso} - S^2_{aniso}$.

Table 1: Ferrocytochrome c_2 Simple Model Free Parameters Derived from ^{15}N Relaxation at 30 °C[a]

residue	S^2	σ	τ_e	σ	residue	S^2	σ	τ_e	σ
D2	0.822	0.007	18.40	4.84	S56	0.812	0.008	17.90	5.65
A3	0.815	0.009	24.50	6.91	A59	0.869	0.007	5.00	5.45
A4	0.79	0.006	28.80	4.11	L60	0.846	0.007	9.20	5.71
K5	0.806	0.009	9.11	5.78	G61	0.881	0.009	25.30	9.45
G6	0.887	0.015	1.44	4.96	A62	0.891	0.006	17.80	7.92
E7	0.852	0.01	6.01	6.44	S63	0.793	0.007	3.34	3.18
K8	0.865	0.012	2.28	4.50	G64	0.854	0.01	4.07	4.75
E9	0.847	0.011	22.70	9.96	A65	0.687	0.006	3.16	1.93
K12	0.835	0.01	20.40	7.90	F66	0.799	0.009	4.01	3.94
C13*	0.739	0.009	15.90	4.14	W67	0.793	0.007	1.77	2.40
K14	0.855	0.01	18.50	8.05	T68	0.712	0.013	1.42	2.27
T15	0.853	0.008	21.50	7.34	E70	0.846	0.008	22.20	7.10
C16*	0.855	0.015	20.40	11.10	I72	0.875	0.01	12.80	9.21
H17*	0.815	0.013	5.68	5.67	T74	0.804	0.009	5.58	5.01
S18	0.739	0.011	4.90	3.82	V76	0.866	0.009	6.00	6.52
I19	0.84	0.013	11.80	8.03	K77	0.892	0.007	7.71	7.08
I20	0.824	0.013	17.00	7.75	D78	0.783	0.005	3.80	3.16
A21	0.853	0.009	12.30	6.61	G80	0.817	0.011	17.90	7.45
D23	0.752	0.007	5.45	3.10	L83	0.869	0.01	6.19	6.76
G24	0.82	0.01	16.10	5.63	K84	0.866	0.01	5.79	6.83
T25	0.817	0.008	9.23	4.89	K86	0.849	0.008	10.80	6.41
E26	0.749	0.007	22.40	3.58	L87	0.843	0.01	5.64	6.12
I27	0.719	0.01	29.40	3.99	D88	0.851	0.009	7.91	5.90
V28	0.807	0.011	3.87	4.62	D89	0.799	0.008	16.70	4.95
K29	0.786	0.008	7.55	4.58	K90	0.779	0.007	12.80	4.27
G30	0.701	0.009	29.50	3.74	A92	0.838	0.007	4.82	4.79
A31	0.712	0.009	12.00	3.47	K93	0.804	0.012	12.20	6.21
K32	0.859	0.019	9.58	10.70	T94	0.754	0.012	22.30	6.26
G34	0.807	0.011	11.30	6.10	M96*	0.836	0.013	0.01	0.11
N36	0.816	0.011	11.80	6.59	A97	0.811	0.011	2.48	3.75
L37	0.83	0.013	28.60	8.07	F98	0.632	0.006	20.80	2.07
Y38	0.887	0.009	11.10	8.62	K99	0.774	0.009	27.20	4.81
G39	0.749	0.008	22.70	3.78	A101	0.809	0.007	25.60	5.28
V40	0.874	0.009	24.00	8.37	K102	0.756	0.007	30.10	4.16
R43	0.854	0.008	25.40	6.72	G104	0.876	0.014	6.36	8.73
T44	0.802	0.008	3.42	3.55	E105	0.866	0.011	45.90	12.90
G46	0.826	0.016	6.55	6.59	D106	0.835	0.011	31.50	9.17
T47	0.859	0.023	3.03	6.84	V107	0.84	0.011	14.70	9.45
Y48	0.836	0.015	6.89	7.16	A108	0.882	0.011	41.20	13.50
E50	0.753	0.009	13.40	4.53	A109	0.864	0.008	17.70	8.19
F51	0.687	0.005	10.70	2.08	Y110	0.835	0.009	33.10	7.03
K52	0.781	0.008	6.36	4.18	S113	0.781	0.007	14.40	4.11
Y53	0.742	0.009	9.15	4.17	V115	0.817	0.007	14.90	5.22
K54	0.831	0.015	6.16	7.43					
D55	0.789	0.007	13.40	4.46					

[a] An axially symmetric model was used to treat global molecular reorientation (see text). Asterisks denote residues that are covalently linked to the heme prosthetic group.

conditions (*2*). A similar $D_\parallel/D_\perp$ ratio of 1.33 was determined though a significantly longer correlation time for global tumbling of 10.4 ns was obtained. However, consideration of the differences in protein concentration and temperature between the two studies suggests that after correction for the resulting differences in viscosity, the results are quantitatively consistent.

The model free squared generalized order parameters (S^2) and local effective correlation times (τ_e) for ferrocytochrome c_2 derived from ^{15}N relaxation obtained assuming axially symmetric tumbling as described above are listed in Table 1. The bulk of the amide N−H S^2 values are near a value of 0.8 (Figure 2a). The corresponding effective correlation times fall in the 1−50 ps range (Figure 3). The obtained model free parameters are generally consistent with a well-ordered polypeptide backbone. There are also several regions of the backbone that fall between regions of regular secondary structure, residues 31 through 33, 51 and 51, 69 and 96, that are characterized by slightly lower order parameters (0.7 ± 0.05). Overall, the backbone dynamics of ferrocytochrome c_2 reveal no systematic differences from values that have been tabulated for global proteins generally or for this protein at a lower temperature (*2*).

Methyl Dynamics Determined from ^{2}H Relaxation. Deuterium NMR relaxation experiments and analysis were carried out as described under Experimental Procedures. A representative example of the CHD_2-selected ^{13}C-HSQC spectrum is shown in Figure 4. Relaxation rates of I_zC_z, $I_zC_zD_z$, and $I_zC_zD_y$ coherences were measured for $^{13}CH_2D$ isotopomers from 48 methyl groups in *R. capsulatus* ferrocytochrome c_2 at static magnetic field strengths of 14.1 and 17.6 T (76.7 and 92 MHz ^{2}H, respectively) at 30 °C. These rates were decomposed into pure ^{2}H longitudinal and transverse rates using eqs 8 and 9 (see Experimental Procedures). Methyl group S^2 and τ_e parameters were obtained via fits to eqs 4−6 and the corresponding methyl symmetry axis squared generalized order parameters (S^2_{axis}) calculated under the assumption of rapid rotation of a methyl group having tetrahedral geometry (*61*) (Table 2). The resulting S^2_{axis} parameters are shown in Figure 5 and the

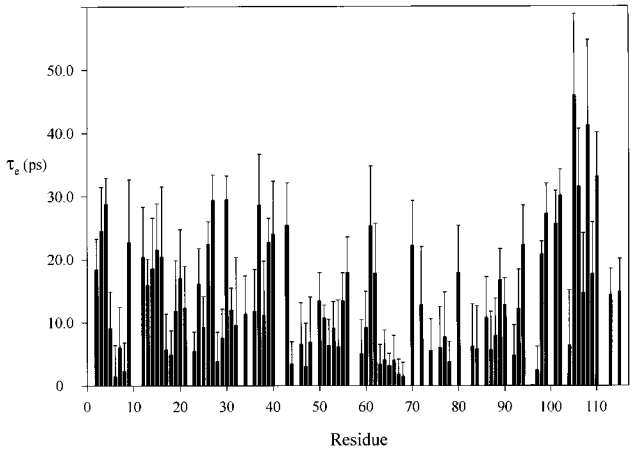

FIGURE 3: Effective correlation time constants for local motion of backbone amide N−H in ferrocytochrome c_2 derived from ^{15}N relaxation data recorded at 30 °C and analyzed using an axially symmetric diffusion tensor (see text).

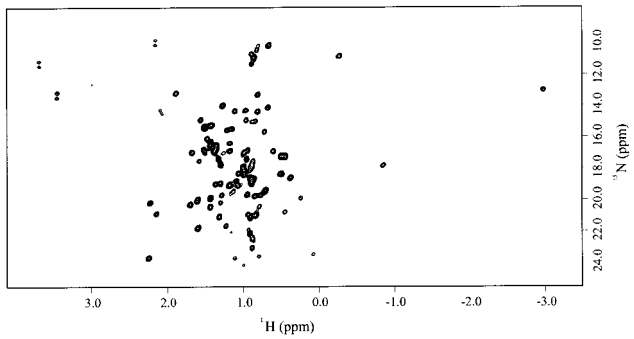

FIGURE 4: ^{13}C-HSQC plane from the ^{13}C $I_zC_zD_z$ relaxation data set recorded for ferrocytochrome c_2 at 92 MHz ^{2}H and 30 °C.

corresponding effective correlation times in Figure 6. Though dominated by the rapid methyl group rotation (*31*), the effective correlation times show considerable heterogeneity indicative of significant variation in the correlation time describing motion of the methyl symmetry axis.

The Interior of Cytochrome c_2 Is Unusually Rigid. The S^2_{axis} values measured for ferrocytochrome c_2 span a wide range, 0.2 to essentially 1.0, indicating a substantial heterogeneity of side chain motion. This heterogeneity, which is a consistent general observation derived from similar investigations of other proteins, stands in rather remarkable contrast to the relatively limited distribution of backbone order parameters derived from ^{15}N relaxation. The two views generate a portrait of protein dynamics which depicts relatively restricted motions for the main chain elements with a comparatively wider range of motion among side chain elements, even for those side chains that are completely buried in the protein interior.

The methyl symmetry axis squared generalized order parameters obtained for ferrocytochrome c_2 are as large as, and in certain cases substantially larger than, averages compiled to date for proteins. Average values for S^2 based on residue types in ferrocytochrome c_2 are: Ala = 0.89 ± 0.19; Ile $\delta1$ = 0.61 ± 0.23; Ile $\gamma2$ = 0.95 ± 0.09; Leu δ = 0.84 ± 0.14; Thr $\gamma2$; Val γ = 0.64 ± 0.23 (*31, 32, 34, 36, 59, 62, 63*). Specifically, although order parameters for alanine β, isoleucine $\delta1$, threonine $\gamma2$, and valine γ are quite similar to published ranges, the ferrocytochrome c_2 S^2_{axis} parameters for isoleucine $\gamma2$ and especially leucine δ methyl groups are substantially higher than currently published ranges. Overall, it appears that ferrocytochrome c_2 is among the most rigid proteins examined to date.

Recently, it has been observed that native proteins tend to partition subnanosecond motion of methyl-bearing side chains into three classes of motion centered on S^2_{axis} values of 0.3, 0.6, and 0.8 (*38*). None of the proteins examined previously using deuterium relaxation methods have large prosthetic groups. The distribution of S^2_{axis} values in ferrocytochrome c_2 reveals the absence of the band centered on ~0.3 (Figure 8) and considerable relative enrichment of the most motionally restricted class of methyl-bearing side chain dynamics centered on an S^2_{axis} value of ~0.85.

Structural Correlates of Side Chain Dynamics. To provide a structural context for interpretation of side chain order parameters, we present a detailed review of the methyl S^2_{axis} values in terms of solvent accessibility, secondary structure elements, and proximity to the heme moiety. Although one does not anticipate that the mere presence of a particular residue or type of residue with a stable secondary structure should generally confer predictable dynamics on the side chains, it is also conceivable that certain structural features may modulate the extent of motions possible for particular side chain elements. Certain fundamental steric constraints are immediately apparent; i.e., the two methyl groups of valine and leucine form an isopropyl moiety, and as expected the γ_1 and γ_2 methyl groups of valine are highly correlated, as are the $\delta1$ and $\delta2$ methyl groups of leucine. Alanine methyl groups tend to reflect the order of the amide N−H of the same residue.

The well-ordered methyl group of alanine-3 (S^2_{axis} = 0.87; S^2_{NH} = 0.82) is wedged in a cleft formed between helix-1, that is formed from N-terminal residues 1−20, and helix-5, which is comprised of C-terminal residues 90−116, and is representative of an alanine methyl group located in stable secondary structure. Interestingly, the relatively flexible alanine-101, which lies on the surface in a loop between helices-4 and -5, has an S^2_{axis} of 0.46. This varies from the usual observation that the flexibility of alanine methyl groups is always correlated with that of the peptide backbone, as in this instance the S^2 value for the alanine-101 amide N−H is 0.82. The γ methyl groups of valine-114 and valine-115, which lie at the end of helix-5, are completely exposed to solvent and have relatively low S^2_{axis} parameters of 0.60 and 0.48, respectively. The S^2_{axis} values for the δ methyl groups of leucine-111 are relatively high (average S^2_{axis} equal to 0.9). This residue is wedged between the edge of the heme porphyrin, the $\delta1$ methyl of leucine-19, and the $\delta1$ methyl of leucine-37 and is also near the helix-1/helix-5 crossing point. There is a conduit of residues with moderate to high methyl order parameters running from leucine-37 and leucine-111 (S^2_{axis} equal to 0.89 and 0.90, respectively), which are close to one another and the heme, to alanine-31 (S^2_{axis} equal to 0.85), then on to isoleucine-19 (S^2_{axis} equal to 0.86 and 0.79 for γ and δ methyl groups, respectively), and ending near isoleucine-27 (γ methyl S^2_{axis} equal to 0.89).

The influence of the heme porphyrin on side chain dynamics seems to defy simple description, as might be derived, for example, by invoking steric constraint. Certainly, the fact that the γ methyl of methionine-96 is coordinated to the iron ion accounts for the high order parameter observed

Table 2: Methyl Symmetry Axis Simple Model Free Parameters of Ferrocytochrome c_2 Derived from ^{2}H Relaxation at 30 °C[a]

	S^2_{axis}	σ	τ_e (ps)	σ	χ^2		S^2_{axis}	σ	τ_e (ps)	σ	χ^2
A3β	0.87	0.06	88.1	4.6	1.1	I72δ1	0.77	0.03	12.5	1.6	0.6
T15γ2	0.27	0.01	67.9	1.2	3.4	I72γ2	1.01	0.04	29.4	1.8	3.7
I19δ1	0.79	0.03	12.4	1.7	1.1	T74γ2	0.70	0.02	49.0	3.1	1.0
I19γ2	0.86	0.06	31.6	2.6	0.4	V76γ	0.80	0.03	33.1	2.8	0.6
I20δ1	0.41	0.02	35.5	1.2	2.6	V76γ	0.80	0.03	29.4	1.9	1.7
I20γ2	0.93	0.03	27.9	1.5	1.5	A81β	0.93	0.06	80.4	5.4	3.1
A21β	0.94	0.04	11.2	1.4	0.1	L83δ	0.86	0.11	32.2	9.3	0.7
T25γ2	0.78	0.04	37.6	2.3	6.6	L87δ	0.59	0.05	62.3	3.5	6.6
I27δ1	0.30	0.01	28.4	0.9	0.2	A92β	0.88	0.04	31.8	2.1	0.5
I27γ2	0.89	0.03	15.9	1.2	1.2	T94γ2	0.89	0.04	13.3	1.9	0.7
A31β	0.85	0.02	13.6	1.2	9.1	M96ϵ	1.05	0.05	5.4	1.7	1.8
T33γ2	0.41	0.02	57.6	1.2	0.7	A97β	0.88	0.04	50.5	2.4	0.6
L37δ	0.89	0.08	20.8	3.7	0.1	L100δ	0.80	0.06	30.4	3.3	0.7
V41γ	0.84	0.02	39.7	2.5	1.1	L100δ	0.86	0.12	49.7	11.2	0.3
T44γ2	0.75	0.12	89.8	7.6	0.9	A101β	0.46	0.01	46.2	0.9	2.6
A45β	1.17	0.05	25.8	2.0	2.4	V107γ	0.31	0.03	78.7	3.8	1.5
T47γ2	0.72	0.08	119	11.2	6.3	V107γ	0.25	0.01	60.9	1.5	1.9
I57δ1	0.75	0.03	7.3	1.6	0.7	A108β	1.05	0.05	59.9	4.6	4.7
I57γ2	1.08	0.11	77.5	10.7	4.6	L111δ	0.80	0.04	30.8	4.5	1.4
V58γ	0.87	0.03	54.7	2.8	0.8	L111δ	0.99	0.15	44.7	6.9	6.7
V58γ	0.93	0.05	24.1	2.2	0.2	V114γ	0.57	0.02	48.9	1.8	0.1
L60δ	0.76	0.07	62.1	6.5	0.2	V114γ	0.64	0.02	36.1	1.6	0.5
L60δ	1.13	0.17	47.3	21.9	0.3	V115γ	0.48	0.01	44.3	1.2	0.4
T68γ2	0.81	0.02	42.3	1.5	1.1	V115γ	0.49	0.01	40.5	1.6	0.6

[a] An axially symmetric model was used to treat global molecular reorientation (see text).

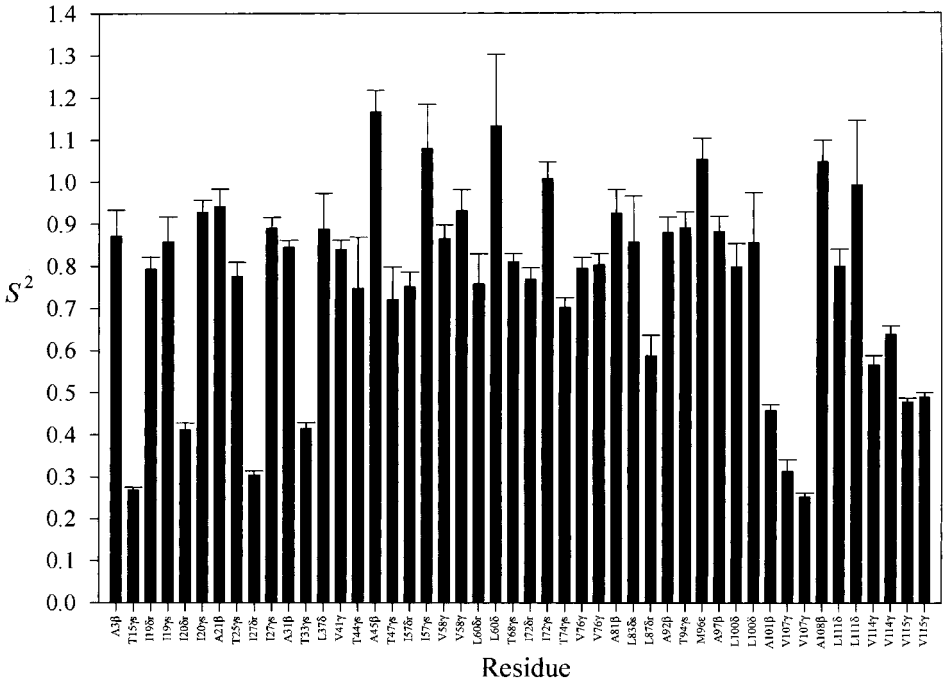

FIGURE 5: Methyl symmetry axis squared generalized order parameters of ferrocytochrome c_2 derived from ^{2}H relaxation recorded at 30 °C.

($S^2_{axis} \sim 1.0$) for this methyl group. In addition, a number of other methyl groups that are located on the methionine side of the heme porphyrin plane display relatively high order parameter values, and include the β methyl groups of alanine-81 and alanine-97 and the γ methyl groups of valine-97 (see Figure 7). Conversely, the methyl groups of valine-107 lie next to the edge of the heme near CMB (methyl-1) and CBB, and are wedged between the heme porphyrin and the crossing of helices- 1 and -5, and yet have relatively low order parameters (average S^2_{axis} equal to 0.28). The γ2 methyl of threonine-15 that is located at the end of helix-1 and is also proximate to the heme at CMC (methyl-3) also has large-amplitude motion (S^2_{axis} equal to 0.27). The γ2 methyl of threonine-33 is located above the heme at the solvent-exposed edge above CMD (methyl-5), and has a relative S^2_{axis} value of 0.41.

Several methyl groups with moderate and higher order parameters are located within a tetragonal region formed in the turn between helix-4 and helix-5 and the heme group. Included in this group are the β methyl of alanine-108 ($S^2_{axis} \sim 1.0$), the γ2 methyl of isoleucine-72 ($S^2_{axis} \sim 1.0$), the δ methyl of leucine-111 (S^2_{axis} of 0.80), the δ methyl of leucine-37 (S^2_{axis} of 0.89), and the γ methyl of valine-76 (S^2_{axis} of 0.80).

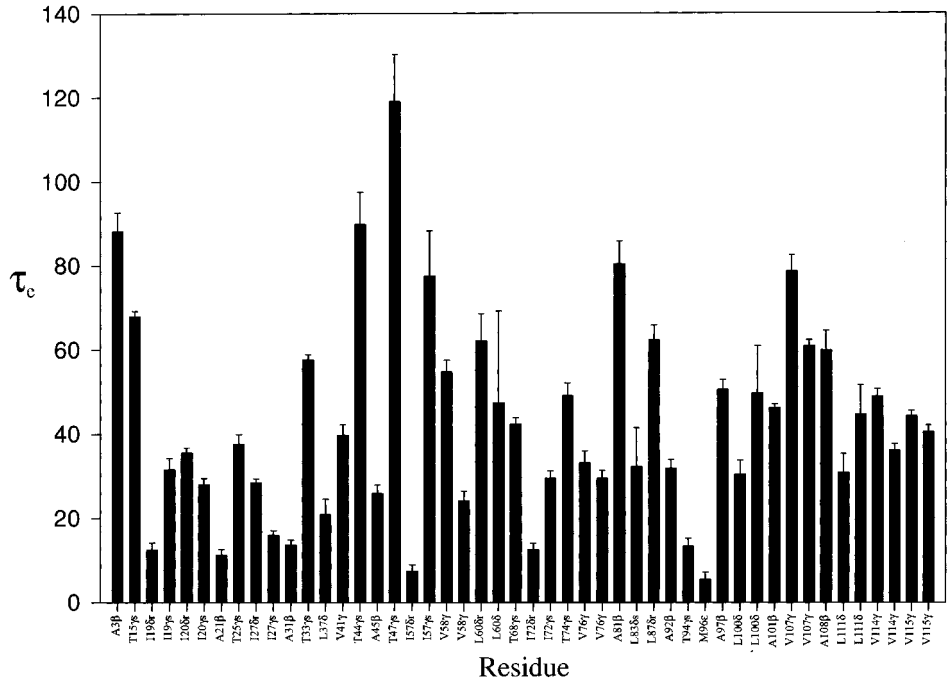

FIGURE 6: Methyl symmetry axis effective correlation time constants of ferrocytochrome c_2 derived from ^{2}H relaxation at 30 °C.

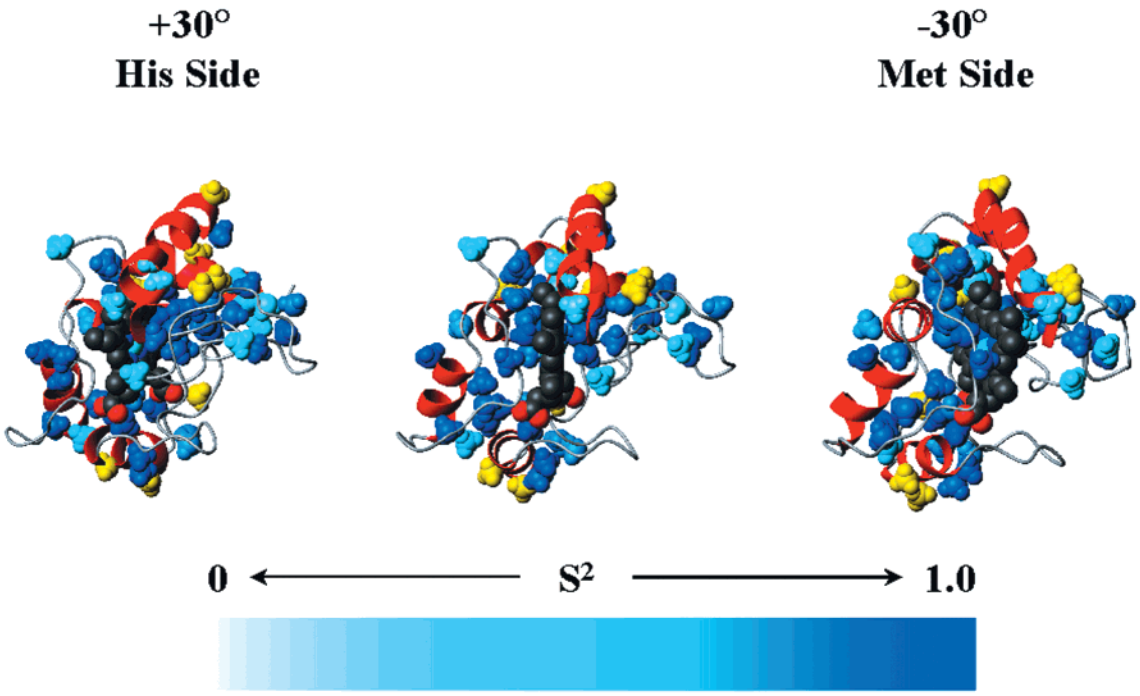

FIGURE 7: Ferrocytochrome c_2 S^2_{axis} parameters colored-coded on the crystal structure [Benning et al. (*1*)].

Based on the preceding analysis, it does not appear that any significant direct relationship between structure and dynamics exists in ferrocytochrome c_2. High methyl squared generalized order parameters are prevalent among all of the secondary structure elements present in the protein. Importantly, the average side chain order in ferrocytochrome c_2 is significantly higher than that seen for previously studied proteins (see Table 2). Nevertheless, relatively low methyl squared generalized order parameters are present as well, such as for V107, which would seem to be rigidly fixed between two helices and the rigid heme moiety. Similarly, no clear relationship between methyl order and solvent-accessible area emerges, and although the bulk of the side chain methyl groups populating the core have relative high order parameters, buried methyl groups with low order exist as well (Table 3). Buried methyl groups exhibiting low order parameters have been noted frequently in previous studies (*30*, *31*, *34*, *62*, *63*). This necessarily requires movement of a number of side chains in order to accommodate significant angular excursions of largely buried methyl-bearing side chains.

Heme Dynamics. Though the deuterium enrichment scheme used was designed to appropriately label side chain methyl groups of amino acids for ^{2}H relaxation analysis, it also resulted in enrichment of the methyl groups of the heme. The ^{1}H and ^{13}C resonances of ferrocytochrome have been

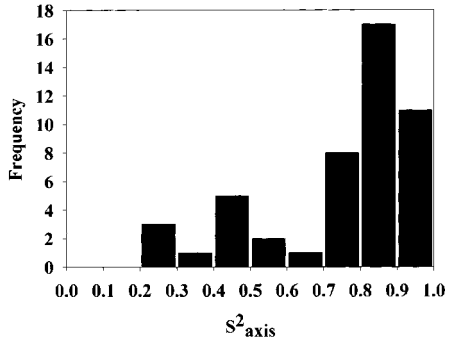

FIGURE 8: Histogram of the distribution of S^2_{axis} parameters in ferrocytochrome c_2.

Table 3: Simple Model Free Parameters of Ferrocytochrome c_2 Derived from ^{2}H Relaxation at 30 °C Compared with Solvent-Accessible Surface Area[a]

methyl	S^2_{axis}	side chain % SAS (Å)	methyl	S^2_{axis}	side chain % SAS (Å)
A3β	0.87	46	I72δ1	0.77	1
T15γ2	0.27	63	I72γ2	1.01	1
I19δ1	0.79	0	T74γ2	0.70	49
I19γ2	0.86	0	V76γ	0.80	1
I20δ1	0.41	23	V76γ	0.80	1
I20γ2	0.93	23	A81β	0.93	58
A21β	0.94	18	L83δ	0.86	0
T25γ2	0.78	55	L87δ	0.59	19
I27δ1	0.30	25	A92β	0.88	0
I27γ2	0.89	25	T94γ2	0.89	21
A31β	0.85	29	M96ϵ	1.05	0
T33γ2	0.41	72	A97β	0.88	25
L37δ	0.89	0	L100δ	0.80	3
V41γ	0.84	23	L100δ	0.86	3
T44γ2	0.75	45	A101β	0.46	88
A45β	1.17	0	V107γ	0.31	1
T47γ2	0.72	43	V107γ	0.25	1
I57δ1	0.75	1	A108β	1.05	1
I57γ2	1.08	1	L111δ	0.80	2
V58γ	0.87	47	L111δ	0.99	2
V58γ	0.93	47	V114γ	0.57	7
L60δ	0.76	3	V114γ	0.64	7
L60δ	1.13	3	V115γ	0.48	29
T68γ2	0.81	54	V115γ	0.49	29

[a] An axially symmetric model was used to treat global molecular reorientation (see text). Solvent-accessible surface areas (SAS) for all side chain atoms are expressed as a percentage of the total surface area.

assigned in previous studies (*20, 21*), which enable us to make direct measurement of heme group dynamics. ^{2}H NMR relaxation data for heme methyl groups were analyzed in a manner identical to that used for the protein side chain methyl groups. The model free parameters for the heme methyl groups of ferrocytochrome c_2 appear in Table 4, and indicate that the heme porphyrin in the reduced form of cytochrome c_2 is highly rigid, with S^2_{axis} values near unity for all measured sites. There is thus no evidence for significant librational motion of the heme.

Implications for Electron Transfer. Protein-mediated electron transfer plays a central role in biology and has accordingly been the focus of significant experiment and theoretical development [for a review, see Moser et al. (*64*)]. Marcus theory provides a remarkable framework within which to describe the character of interprotein electron transfer (*65*). In the weak coupling limit, the rate of electron transfer is the product of the square of the electronic coupling between donor and acceptor and the probability of the donor and acceptor forming a resonant activated complex. Though

Table 4: Simple Model Free Parameters for the Heme Methyl Groups of Ferrocytochrome c_2 Derived from ^{2}H Relaxation at 30 °C[a]

		S_2^{axis}	σ	τ_e	σ
methyl-1	CMB	0.92	0.10	6.6	5.8
methyl-3	CMC	0.99	0.06	15.1	2.1
methyl-5	CMD	1.20	0.29	1.9	5.6
methyl-8	CMA	0.92	0.09	3.6	5.0

[a] Obtained using an axially symmetric diffusion tensor for global tumbling. Heme methyl nomenclature according to Mathews (*74*) is given in the first column, and the alternative convention of Benning et al. (*1*) is given in the second column.

the relevance to the *evolution* of electron-transfer chains in biology has been disputed (*66*), the underlying origin of the electronic coupling in terms of dominant pathways of electron tunneling in proteins is clearly of fundamental interest (*67*). Using the photosynthetic reaction center as a model, Balabin and Onuchic (*43*) have recently elaborated the pathways of treatment to include the effects of protein dynamics. This extension indicates that when an electron-transfer process is dominated by a single pathway "tube" corrections due to protein dynamics are minor. However, when multiple pathways exist, the electronic coupling is sensitive to conformational dynamics such that the dominant tunneling pathways occur in protein conformations significantly removed from the equilibrium structure. The unusual rigidity of ferrocytochrome c_2 would appear to significantly reduce the importance of the latter mechanism for electron transfer from the reduced state of this heme protein. Furthermore, a rigid protein environment is fully consistent with the small reorganization energy suggested by theoretical analysis of other redox proteins (*41, 42*). Confirmation of this view must, however, await characterization of the dynamics of the oxidized redox state of the protein. Such studies are in progress.

Implications for Protein Design. Over the past decade, *de novo* protein design has progressed from the design of folded monomeric helices to large-scale globular proteins with well-defined hydrophobic cores (*68*). Protein design serves as a powerful arena for testing our understanding of the fundamental principles of protein structure and function. Designed heme proteins also provide a powerful vehicle with which to explore the fundamental interactions between protein and prosthetic group and thereby complement studies with natural proteins (*44, 69, 70*). Roberston et al. (*44*) introduced multiheme synthetic proteins based on a helix−disulfide−helix monomer architecture. These (α-SS-α) units self-associate to yield four α-helix bundles with either two or four heme binding sites. Although high-affinity binding and appropriate redox chemistry are achieved, the structural quality of the heme−protein complex is limited, as evidenced by extensive dynamic averaging in their NMR spectra (*44*). In contrast, the apostates of such peptide assemblies are well structured [e.g., Skalicky et al. (*71*)]. Thus, one must conclude that the structural criteria necessary to attain a precisely structured heme−protein complex are remarkably stringent.

Interestingly, Handel and co-workers have investigated the effects of core (hydrophobic) packing on side chain dynamics in ubiquitin (*72, 73*). The core residues of the protein were extensively mutated in a redesign effort, and though the

resulting protein had the same fold, the precise distribution of fast internal dynamics was extensively different. These results indicate that multiple distributions of core dynamics are compatible with a particular global structure and stability of proteins lacking large prosthetic groups. In contrast, the results obtained for ferrocytochrome c_2 would seem to indicate that there is little malleability in the protein−heme interface and correspondingly little room for error in the design of such complexes.

ACKNOWLEDGMENT

We thank Professor Fevzi Daldal for providing a plasmid harboring the gene for cytochrome c_2 and for advice during the initial stages of this work. We gratefully acknowledge the help of Hong Lin and Lynne Grazianni for preparation of the isotopically enriched ferrocytochrome c_2 samples used in the study.

REFERENCES

1. Benning, M. M., Wesenberg, G., Caffrey, M., Bartsch, R. G., Meyer, T. E., Cusanovich, M. A., Rayment, I., and Holden, H. (1991) *J. Mol. Biol. 281*, 341−361.
2. Cordier, F. Caffrey, M., Brutscher, B., Cusanovich, M. A., Marion, D., and Blackledge, M. (1998) *J. Mol. Biol. 281*, 341−361.
3. Ulmer, D. D., and Kagi, J. H. R. (1968) *Biochemistry 7*, 2710−2717.
4. Patel, D. J., and Canuel, L. L. (1976) *Proc. Natl. Acad. Sci. U.S.A. 73*, 1398−1402.
5. Osheroff, N., Borden, D., Koppenol, W. H., and Margoliash, E. (1980) *J. Biol. Chem. 255*, 1689−1697.
6. Eden, D., Matthew, J. B., Rosa, J. J., and Richards, F. M. (1982) *Proc. Natl. Acad. Sci. U.S.A. 79*, 815−819.
7. Wand, A. J., Roder, H., and Englander, S. W. (1986) *Biochemistry 25*, 1107−1114.
8. Arean, C. O., Moore, G. R., Williams, G., and Williams, R. J. P. (1988) *Eur. J. Biochem. 173*, 607−615.
9. Trewhella, J., Carlson, V. A. P., Curtis, E. H., and Heidorn, D. B. (1988) *Biochemistry 27*, 1121−1125.
10. Milne, J. S., Mayne, L., Roder, H., Wand, A. J., and Englander, S. W. (1998) *Protein Sci. 7*, 739−745.
11. Takano, T., and Dickerson, R. E. (1981) *J. Mol. Biol. 153*, 79−94.
12. Takano, T., and Dickerson, R. E. (1981) *J. Mol. Biol. 153*, 95−115.
13. Berghuis, A. M., and Brayer, G. D. (1992) *J. Mol. Biol. 223*, 959−976.
14. Feng, Y., Roder, H., and Englander, S. W. (1990) *Biochemistry 29*, 3494−3504.
15. Qi, P. X., Di Stefano, D. L., and Wand, A. J. (1994) *Biochemistry 33*, 6408−6417.
16. Qi, P. X., Beckman, R. A., and Wand, A. J. (1996) *Biochemistry 35*, 12275−12286.
17. Banci, L., Bertini, I., Huber, J. G., Spyroulias, G. A., and Turano, P. (1999) *J. Biol. Inorg. Chem. 4*, 21−31.
18. Gooley, P. R., Caffrey, M. S., Cusanovich, M., and MacKenzie, N. E. (1990) *Biochemistry 29*, 2278−2290.
19. Gooley, P. R., and MacKenzie, N. E. (1990) *FEBS Lett. 2*, 225−228.
20. Gooley, P. R., Zhao, D., and MacKenzie, N. E. (1991) *J. Biomol. NMR 1*, 145−154.
21. Caffrey, M., Brutscher, B., Simorre, J. P., Fitch, J., Cusanovich, M. A., and Marion, D. (1994) *Eur. J. Biochem. 221*, 63−75.
22. Kay, L. E., Torchia, D. A., and Bax A. (1989) *Biochemistry 28*, 8972−8979.
23. Dellwo, M. J., and Wand, A. J. (1989) *J. Am. Chem. Soc. 111*, 4571−4578.
24. Clore, G. M., Szabo, A., Bax, A., Kay, L. E., Driscoll, P. C., and Gronenborn, A. M. (1990) *J. Am. Chem. Soc. 112*, 4989−4991.
25. Schneider, D. M., Dellwo, M. J., and Wand, A. J. (1992) *Biochemistry 31*, 3645−3652.
26. Stone, M. J., Fairbrother, W. J., Palmer, A. G., III, Reizer, J., Saier, M. H., Jr., and Wright, P. E. (1992) *Biochemistry 31*, 4394−4406.
27. Mandel, A. M., Akke, M., and Palmer, A. G., III (1995) *J. Mol. Biol. 246*, 144−163.
28. Dayie, K. T., and Wagner, G. (1997) *J. Am. Chem. Soc. 119*, 7797−7806.
29. Le Master, D. M., and Kushlan, D. M. (1996) *J. Am. Chem. Soc. 118*, 9263−9272.
30. Wand, A. J., Urbauer, J. L., McEvoy, R. P., and Beiber, R. J. (1996) *Biochemistry 35*, 6116−6125.
31. Lee, A. L., Flynn, P. F., and Wand A. J. (1999) *J. Am. Chem. Soc. 121*, 2891−2902.
32. Muhandiram, D. R., Yamazaki, T., Sykes, B. D., and Kay, L. E. (1995) *J. Am. Chem. Soc. 117*, 11536−11544.
33. Nicholson, L. K., Kay, L. E., Baldisseri, D. M., Arango, J., Young, P. E., Bax, A., and Torchia, D. A. (1992) *Biochemistry 31*, 5253−5263.
34. Constantine, K. L., Friedrichs, M. S., Wittekind, M., Jamil, H., Chu, C. H., Parker, R. A., Goldfarb, V., Mueller, L., and Farmer, B. T., III (1998) *Biochemistry 37*, 7965−7980.
35. Le Master, D. M. (1999) *J. Am. Chem. Soc. 121*, 1726−1742.
36. Mittermaier, A., Kay, L. E., and Forman-Kay, J. D. (1999) *J. Biomol. NMR 13*, 181−185.
37. Lee, A. L., Kinnear, S. A., and Wand, A. J. (2000) *Nat. Struct. Biol. 7*, 72−77.
38. Lee, A. L., and Wand, A. J. (2001) *Nature*, in press.
39. Li, Z., Raychaudhuri, S., and Wand, A. J. (1996) *Protein Sci. 5*, 2647−2650.
40. Yang, D., and Kay, L. E. (1996) *J. Mol. Biol. 263*, 369−382.
41. Muegge, I., Qi, P. X., Wand, A. J., Chu, Z. T., and Warshel, A. (1997) *J. Phys. Chem. B 101*, 825−836.
42. Parson, W. W., Chu, Z. T., and Warshel, A. (1998) *Biophys. J. 74*, 182−191.
43. Balabin, I. A., and Onuchic, J. N. (2000) *Science 290*, 114−118.
44. Robertson, D. E., Farid, R. S., Moser, C. C., Urbauer, J. L., Mulholland, S. E., Pidikiti, R., Lear, J. D., Wand, A. J., DeGrado, W. F., and Dutton, P. L. (1994) *Nature 368*, 425−432.
45. Raiford, D. S., Fisk, C. L., and Becker, E. D. (1979) *Anal. Chem. 51*, 2050−2051.
46. Neri, D., Szyperski, T., Otting, G., Senn, H., and Wüthrich, K. (1989) *Biochemistry 28*, 7510−7516.
47. Nirmala, N. R., and Wagner, G. (1988) *J. Am. Chem. Soc. 110*, 7557−7558.
48. Palmer, A. G., III, Skelton, N. J., Chazin, W. J., Wright, P. E., and Rance, M. (1992) *Mol. Phys. 75*, 699−711.
49. Sklenar, V., Torchia, D., and Bax, A. (1987) *J. Magn. Reson. 73*, 375−379.
50. Farrow, N. A., Muhandiram, R., Singer, A. U., Pascal, S. M., Kay, C. M., Gish, G., Shoelson, S. E., Pawson, T., Forman-Kay, J. D., and Kay, L. E. (1994) *Biochemistry 33*, 5984−6003.
51. Abragam, A. (1961) *Principles of nuclear magnetism*, 1st ed., Oxford University Press, New York.
52. Wittebort, R. J., and Szabo, A. (1978) *J. Chem. Phys. 69*, 1722−1736.
53. Spiess, H. W. (1978) *NMR 15*, 55−214.
54. Lipari, G., and Szabo, A. (1982) *J. Am. Chem. Soc. 104*, 4546−4559.
55. Lipari, G., and Szabo, A. (1982) *J. Am. Chem. Soc. 104*, 4559−4570.
56. Tjandra, N., Feller, S., Pastor, R. W., and Bax, A. (1995) *J. Am. Chem. Soc. 117*, 12562−12566.
57. Mantsch, H. H., Saito, H., and Smith, I. C. P. (1977) *Prog. NMR Spectrosc. 11*, 211−271.
58. Schurr, J. M., Babcock, H. P., and Fujimoto, B. (1994) *J. Magn. Reson. 105B*, 211−214.
59. Lee, L. K., Rance, M., Chazin, W. J., and Palmer, A. G., III (1997) *J. Biomol. NMR 9*, 287−298.

60. Lee, A. L., and Wand, A. J. (1999) *J. Biomol. NMR 13*, 101−112.
61. Woessner, D. E. (1962) *J. Chem. Phys. 37*, 647−654.
62. Kay, L. E., Muhandiram, D. R., Farrow, N. A., Aubin, Y., and Forman-Kay, J. D. (1996) *Biochemistry 35*, 361−368.
63. Gagné, S. M., Tsuda, S., Spyracopoulos, L., Kay, L. E., and Sykes, B. D. (1998) *J. Mol. Biol. 278*, 667−686.
64. Moser, C. C., Keske, J. M., Warncke, K., Farid, R. S., and Dutton, P. L. (1992) *Nature 355*, 796−802.
65. Marcus, R. A., and Sutin, N. (1985) *Biochim. Biophys. Acta 811*, 265−322.
66. Page, C. C., Moser, C. C., Chen, X., and Dutton, P. L. (1999) *Nature 402*, 47−52.
67. Betts, J. N., Beratan, D. N., and Onuchic, J. N. (1992) *J. Am. Chem. Soc. 114*, 4043−4046.
68. DeGrado, W. F., Summa, C. M., Pavone, V., Nastri, F., and Lombardi, A. (1999) *Annu. Rev. Biochem. 68*, 779−819.
69. Choma, C. T., Lear, J. D., Nelson, M. J., Dutton, P. L., Robertson, D. E., and DeGrado, W. F. (1994) *J. Am. Chem. Soc. 116*, 856−865.
70. Gibney, B. R., and Dutton, P. L. (2001) *Adv. Inorg. Chem. 51*, 409−455.
71. Skalicky, J. J., Gibney, B. R., Rabanal, F., Bieber Urbauer, R. J., Dutton, P. L., and Wand, A. J. (1999) *J. Am. Chem. Soc. 121*, 4941−4951.
72. Johnson, E. C., Lazar, G. A., Desjarlais, J. R., and Handel, T. M. (1999) *Struct. Fold. Des. 7*, 967−976.
73. Johnson, E. C., and Handel, T. M. (1999) *J. Biomol. NMR 15*, 135−143.
74. Mathews, F. S. (1985) *Prog. Biophys. Mol. Biol. 45*, 1−56.

BI0102252